



Ultimate Longitudinal Strength Analysis of a Double Skin Tanker by Idealized Structural Unit Method

J.K. Paik, Pusan National University, Pusan, Korea

ABSTRACT

In this study, midship section of a double skin tanker at 280,000 dwt is designed. In order to make a system safety assessment of this hull girder in the longitudinal strength point of view, idealized structural unit method is applied such that the progressive collapse behaviour under sagging or hogging bending moment is efficiently analyzed. For this purpose, an idealized plate element subjected to biaxial load is developed taking account of the influence of initial imperfections as well as the interaction effect between local and global buckling in the structure. A parametric analysis with varying the magnitude of initial imperfections is carried out. Based on the results obtained here, a system safety assessment is made using the conventional measure of safety such as reserve strength factor and safety index. From the results of the present study, the following conclusion is made :

i) the initial imperfections existing in the local plate element reduce the ultimate longitudinal bending moment of ship's hull girder.

ii) the double skin hull girder designed in this study is considered to have a sufficient safety in the longitudinal strength point of view, and

iii) the present method is useful when ultimate collapse strength-based safety assessment or optimization, is made in the structural design stage for a new type of hull girder.

INTRODUCTION

Recently, in order to minimize the risk of ocean pollution due to cargo oil leakage in the event of accidents such as grounding or collision, the needs for construction of a double skin type of hull structure based on a new design concept are increasing in tanker industry[1,2]. Also, for achieving more reliable and economical design of structures, a system safety assessment which refers to the redundancy of the overall structure becomes of great interest[3]. In general, the procedure of system safety assessment of structures is split into two categories : one is a deterministic approach and another is

probabilistic one. The former measures deterministically the margin between the ultimate capacity of the overall structure and the applied loads. In the latter approach, reliability or probability of failure of the structure is evaluated, in which each design parameter is treated as a random variable. For both approaches, however, the key issue is to obtain the ultimate collapse strength of the overall structure under external loading. Here, in order to determine a more reasonable layout of each structural member, structural designer is preferable to have understanding of detail progressive collapse history as well as ultimate collapse capacity.

In usual, ship's strength for the overall structure is classified in three categories such as longitudinal strength, transverse strength and torsional strength. Thus if designers are going to make a system safety assessment of ship's hull girder in the longitudinal strength point of view, then they should perform the ultimate longitudinal bending strength analysis of ship's hull girder subjected to sagging or hogging bending moment. With the increasing of the external bending moment, however, ship's hull girder exhibits highly complicated nonlinear behaviour associated with geometric and material nonlinearity. Also since ship structures are fabricated by heating process such as welding, flame cutting and so on, initial imperfections in the form of initial deflection and residual stress are always present in the structural members and these make structural behaviour more complex one.

For the nonlinear analysis of structure, finite element method(FEM) is one of the most powerful approach. However, a direct application of the conventional FEM to the ultimate longitudinal strength analysis of ship's hull girder which is very large and complex structure is considered to be nearly impossible because a tremendous amount of human labor and computational efforts is required. Therefore, many structural designers or analyzers have a great interest about how to reduce the computing time needed in the nonlinear analysis of structures while gaining the reliable solution. In this respect, Ueda and Rashed[4] proposed an

efficient and accurate numerical method for the nonlinear analysis of large size structures, named idealized structural unit method (ISUM). The main idea behind this methodology is in modelling the objective structure to be analyzed by using very large size structural element, named idealized structural element, comparing with the conventional finite element, which results in the considerable reduction of the computational efforts because the number of unknowns in structural stiffness equation is greatly decreased. In general, for the analysis of a certain type of structure, various kinds of the idealized structural element formulated in advance are needed like in the conventional FEM. Usually each basic structural member composing the objective structure to be analyzed is chosen as an idealized structural element. By idealizing and formulating the nonlinear behaviour of the actual structural member, an idealized structural element is developed. Through many application examples of ISUM to various types of steel structures such as transverse rings [4,5], upper decks [6,7], double bottom structures [8-10], hull girder [11-13] and tubular offshore structures [14-21], it is well known that ISUM is a very powerful and useful methodology for the nonlinear analysis of large size steel structures.

In this study, midship section of a double skin hull structure at 280,000 dwt is designed and in order to make an ultimate longitudinal strength-based system safety assessment of this hull girder, ISUM is applied such that the progressive collapse behaviour under sagging or hogging bending moment is efficiently analyzed. For this purpose, an idealized plate element subjected to biaxial load is formulated taking account of geometric and material nonlinearity. The interaction effect between local and global buckling in the structure is taken into consideration. Also, the influence of initial imperfections in the form of initial deflection and residual stress on strength and stiffness of the structure is considered. A computer program, ALPS/ISUM [22] is completed based on the present theory. A verification of the present theory is made comparing the present solution with the existing numerical and experimental result for unit plate member and welded box-girder. Then the present method is applied to the ultimate longitudinal strength analysis of the example double skin hull girder. A parametric analysis varying the magnitude of initial imperfections is carried out. The reserve strength factor and safety index are evaluated on the basis of the ultimate longitudinal bending strength obtained here.

DESIGN OF MIDSHIP SECTION OF A DOUBLE SKIN HULL GIRDER

Midship section of a double skin tanker at 280,000 dwt is designed. Principal particulars of the ship is 310 m in length, 56.85 m in breadth and 31 m in depth. Also

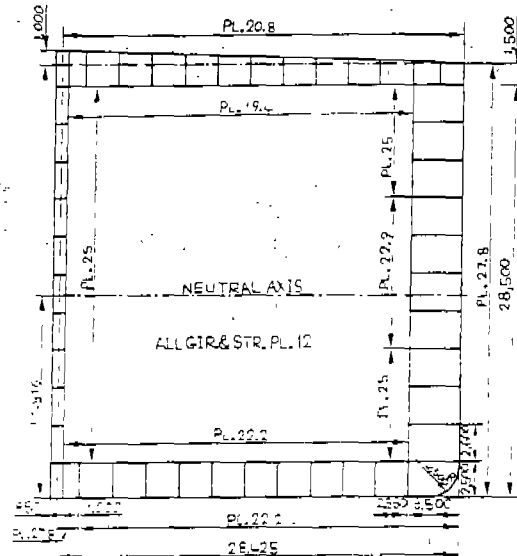


Fig.1 Midship section of a 280K double skin hull structure

the draught is 21 m. The ship has eight cargo tanks having a hull form of double-skinned bottom, side and deck. The longitudinal bulkhead located at center line and the transverse bulkhead between cargo tanks have also a double-skinned structure. The longitudinal girder is arranged in double skin deck and double bottom. Stringer is installed in double side structure and the longitudinal bulkhead. In the present tanker, however, no floor members are arranged and all the plate members have no stiffeners in the longitudinal as well as transverse direction. The detail midship section of the ship is shown in Fig.1. The length of a standard cargo tank is 24 m and transverse space is 5 m. The double bottom depth and side-skin width are 2.5 m and 3.5 m, respectively. For simplicity, all structural members are considered to be built of 36HT high-tensile steel whose yield stress is 36 kg/mm². The section modulus of the present scantling at midship section is checked being greater than the required one from the existing rule of classification societies. The present double skin type of oil tanker is considered to have merits in prevention of oil pollution, cargo oil handling, maintenance of cargo oil quality and so on.

MEASURE OF SYSTEM SAFETY

Based on the ultimate longitudinal bending strength obtained in this study, a system safety assessment is made using two kinds of measure of safety such as reserve strength factor and safety index which are defined as :

$$\gamma = \frac{M_{ult}}{M_{ext}} \quad (1)$$

$$\beta = \frac{\bar{M}_{ult} - \bar{M}_e - \bar{M}_w}{\sqrt{S_{ult}^2 + S_e^2 + S_w^2}} \quad (2)$$

where, γ : reserve strength factor
 β : safety index
 \bar{M}_{ult} : mean of the ultimate longitudinal bending strength
 \bar{M}_{ext} : mean of the total external bending moment ($=\bar{M}_e + \bar{M}_w$)
 \bar{M}_e : mean of the still water bending moment
 \bar{M}_w : mean of the wave-induced bending moment
 S_{ult}, S_e, S_w : standard deviation of the ultimate longitudinal bending strength, the still water bending moment and the wave-induced bending moment, respectively

In the above equation, \bar{M}_{ult} is calculated by ISUM formulated in this study and also \bar{M}_e and \bar{M}_w are estimated by [23]

$$\begin{aligned} \bar{M}_e &= 2/3 M_e \\ \bar{M}_w &= 2/3 M_w \end{aligned} \quad (3)$$

where, M_e and M_w are the still water and the wave-induced bending moment estimated by using the existing rule of a classification society, respectively, in which ABS rule [24] is employed in the present assessment.

Also each standard deviation is calculated by using coefficient of variation (COV) as

$$\begin{aligned} S_{ult} &= COV_{ult} \bar{M}_{ult} \\ S_e &= COV_e \bar{M}_e \\ S_w &= COV_w \bar{M}_w \end{aligned} \quad (4)$$

where, COV_{ult} , COV_e and COV_w denote coefficients of variation for the ultimate longitudinal bending strength, the still water bending moment and the wave-induced bending moment, respectively. In the present analysis, each COV is assumed to be 10%, 10% and 20% for COV_{ult} , COV_e and COV_w , respectively.

THEORY OF ULTIMATE LONGITUDINAL BENDING STRENGTH ANALYSIS BY ISUM

Basic Assumptions

The ship hull girder designed in this study consists of only plate members in deck, bottom and side structure. Longitudinal girder and side stringer are also considered to be plate member. As indicated in Fig.2, each plate member composing the hull girder is treated as unit element which is called an idealized plate element.

In general, the plate element in ship structures is subjected to in-plane and lateral loads. But only in-plane loads are taken into consideration in the present study. The longitudinal compression or tension by the acting of sagging or hogging bending moment on the hull girder is developed in the element. The interaction movement between the adjacent plate elements

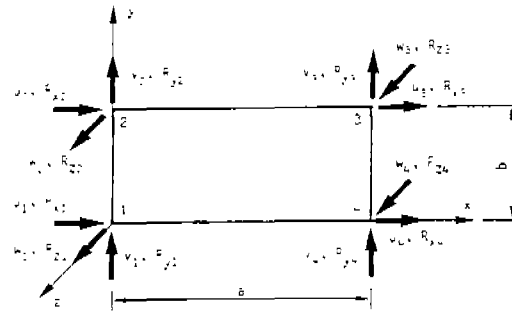


Fig.2 Nodal forces and nodal displacements of the idealized plate element

develops the transverse compression or tension. The magnitude of the shearing force is supposed to be very small in the present problem that the hull girder is under the action of vertical bending moment such that no occurrence of shear buckling in plate element is expected. Thus the dominant components of the external load acting on the plate element are considered to be biaxial loads, as shown in Fig.3. The boundary condition of the plate element is assumed to be simply supported and the edges remain straight even after the lateral deflection is occurred.

The initial imperfections in the form of initial deflection and welding residual stress are always present in real plate element. The actual shape of the initial deflection of the panel is very complex as shown in Fig.3 but for simplicity two kinds of the simplified shape of the initial deflection existing in the plate element are assumed as indicated in Fig.4. Fig.4.a indicates the case that the shape of the initial deflection matches the buckling mode of the plate, while a simplified form of "hungry horse's back" is given in Fig.4.b. The configuration of the initial deflection is depicted by Fourier series function having sufficient terms of the half-wave number. The distribution of the welding residual stress can be idealized as described in Fig.3.

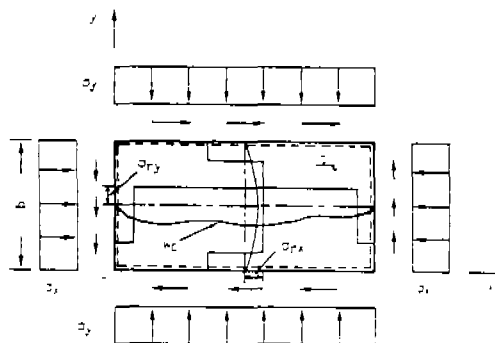


Fig.3 Configuration of the rectangular plate element

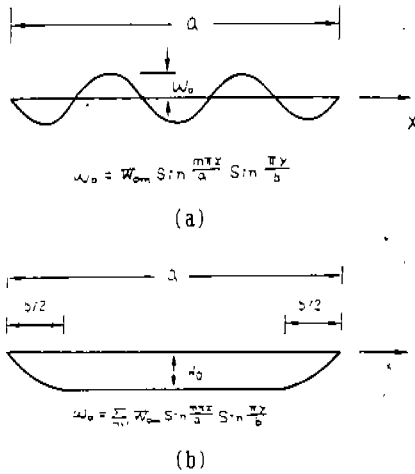


Fig.4 The simplified shape of the initial deflection existing in plate element

There are several types of the limit state in steel structures but the present study considers only the ultimate collapse strength associated with the large deflection and yielding of the plate. In addition, three basic assumptions are made in this study. First, the dynamic loading is treated by the equivalent static one such that the hull girder is considered to be subjected to only static loading. Second, the external loads are proportionally applied. Third, the influence of the lateral loads on the behaviour of plate element itself is not accounted for.

Formulation of Idealized Plate Element Under Biaxial Load

Nodal Forces and Nodal Displacements of the Element. As described in the previous section, very large size plate member which is basic structural component in the structure is chosen as unit element in the present study, see Fig.2. The present study attempts to replace the deflected plate with an equivalent flat plate which has zero deflection by evaluating the reduction of in-plane stiffness due to lateral deflection in advance. Thus rotational degree of freedom in the element becomes to be removed. Then the behaviour of the present plate element is expressed by the nodal force vector $\{R\}$ and the nodal displacement vector $\{U\}$ having three degrees of freedom at each corner nodal point of the element.

$$\{R\} = \{ R_{x1} \ R_{y1} \ R_{z1} \ R_{x2} \ R_{y2} \ R_{z2} \ R_{x3} \ R_{y3} \ R_{z3} \ R_{x4} \ R_{y4} \ R_{z4} \}^T$$

$$\{U\} = \{ u_1 \ v_1 \ w_1 \ u_2 \ v_2 \ w_2 \ u_3 \ v_3 \ w_3 \ u_4 \ v_4 \ w_4 \}^T \quad (5)$$

where, R_x , R_y and R_z indicate axial forces in x, y and z direction and u, v and w denote displacements in x, y and z direction, respectively.

Strain-Displacement relation. In order

to take account of the interaction effect between local and overall buckling in the structure, geometric nonlinear behaviour of the plate element should be considered. The incremental expression of the relationship between the strain and displacement taking account of the large deflection effect of the element is emerged by the following matrix form.

$$\{\Delta \epsilon\} = [B_p]\{\Delta U\} + [C][G]\{\Delta U\} + 1/2[\Delta C][G]\{\Delta U\} \quad (6)$$

where, $\{\Delta \epsilon\} = \{\Delta \epsilon_x \ \Delta \epsilon_y \ \Delta \gamma_{xy}\}^T$: increment of strain components

$$\{\Delta U\} = \{\Delta u_1 \ \Delta v_1 \ \Delta w_1 \ \Delta u_2 \ \Delta v_2 \ \Delta w_2 \ \Delta u_3 \ \Delta v_3 \ \Delta w_3 \ \Delta u_4 \ \Delta v_4 \ \Delta w_4\}^T$$

$$[B_p]\{\Delta U\} = \{\Delta u_{,x} \ \Delta v_{,y} \ \Delta u_{,y} + \Delta v_{,x}\}^T$$

$$[G]\{\Delta U\} = \{\Delta w_{,x} \ \Delta w_{,y}\}^T$$

$$[C] = \begin{bmatrix} w_{,x} & 0 \\ 0 & w_{,y} \\ w_{,y} & w_{,x} \end{bmatrix}$$

Average Stress-Strain Relation of Deflected Plate Element in Elastic Range.

In the real plate element, the initial deflection are always present. The in-plane stiffness of the initially deflected plate decreases gradually from the beginning as the compressive load increases. In the present study, the deflected plate is replaced by an equivalent flat plate which has zero deflection. For this purpose the reduction of the in-plane stiffness due to the existence of the lateral deflection is analytically evaluated in advance.

Fig.5 represents a typical membrane stress distribution of deflected plate under the action of the axial compression. Since the edges of the element is considered to remain straight, the average axial displacements in the longitudinal and transverse direction are calculated by

$$\delta_x = \int \epsilon_x |_{y=0 \text{ or } b} dx = \int (1/E \cdot \sigma_x |_{y=0 \text{ or } b} - \nu/E \cdot \sigma_y |_{y=0 \text{ or } b}) dx$$

$$\delta_y = \int \epsilon_y |_{x=0 \text{ or } a} dy = \int (1/E \cdot \sigma_y |_{x=0 \text{ or } a} - \nu/E \cdot \sigma_x |_{x=0 \text{ or } a}) dy \quad (7)$$

where δ_x and δ_y denote the average axial displacements in x and y direction, respectively. Also E is Young's modulus and ν is Poisson's ratio.

The integration for the stress distribution in Eq.(7) is made along the length or breadth of the element and the result is defined by

$$\int \sigma_x |_{y=0 \text{ or } b} dx = a \cdot \sigma_{x\max}$$

$$\int \sigma_y |_{x=0 \text{ or } a} dy = a \cdot \sigma_{y\max}$$

$$\int \sigma_x |_{x=0 \text{ or } a} dy = b \cdot \sigma_{x\max}$$

$$\int \sigma_y |_{y=0 \text{ or } b} dx = b \cdot \sigma_{y\max} \quad (8)$$

where, $\sigma_{x\max}$ and $\sigma_{y\max}$ are the average membrane stresses of the element in x and y direction, respectively. Also $\sigma_{x\max}$ and $\sigma_{y\max}$ denote the maximum membrane stresses that are developed in the corner of the deflected plate as shown in Fig.5.

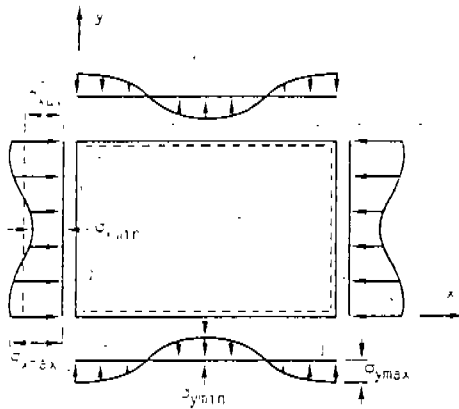


Fig.5 Membrane stress distribution of the deflected plate subjected to axial compression

Substituting Eq.(8) into Eq.(7) and dividing each term in both hand sides of Eq.(7) by length or breadth of the element, the average membrane strain components in x and y direction are given as :

$$\begin{aligned} \epsilon_{xav} &= \delta_x/a = 1/E \cdot \sigma_{xmax} - \nu/E \cdot \sigma_{yav} \\ \epsilon_{yav} &= \delta_y/b = -\nu/E \cdot \sigma_{yav} + 1/E \cdot \sigma_{ymax} \end{aligned} \quad (9)$$

where, ϵ_{xav} and ϵ_{yav} denote the average membrane strain components of the deflected plate in x and y direction, respectively.

On the other hand, since the magnitude of the shearing force acting on the plate element under consideration is very small and the shearing deformation is supposed to be linear, the average shearing strain of the element reads

$$\gamma_{xyav} = 2(1+\nu)/E \cdot \tau_{xyav} \quad (10)$$

where, γ_{xyav} and τ_{xyav} are the average shear strain and stress, respectively.

The maximum membrane stresses σ_{xmax} and σ_{ymax} in Eq.(9) can be calculated by solving the governing equation of the plate element taking account of the initial imperfections. As mentioned in the previous section, since the dominant loading components acting on the plate element are biaxial load and the occurrence of the shear buckling is not expected, the governing equation of the element which is subjected to the biaxial load is directly solved in this study. The shape of the initial deflection of the plate element takes the following form using Fourier series function.

$$w_0 = \sum W_{0m} \sin(m\pi x/a) \sin(n\pi y/b) \quad (11)$$

where, the subscript zero indicates the initial configuration and W_{0m} represents the known coefficient for the initial deflection. Also, the shape of the added deflection of

the plate takes the same form with that of the initial geometry.

$$w = \sum W_m \sin(m\pi x/a) \sin(n\pi y/b) \quad (12)$$

where, W_m indicates the unknown coefficient for the added deflection.

It is known that the large deflection behaviour of the plate element is mainly governed by the half-wave component for the buckling mode [6,25]. Thus, the other terms in Eqs.(11) and (12) except for the buckling mode component may be removed. Therefore, the present study selects only the buckling mode component as the deflection parameter when solving the governing equation so that the summation symbol in Eqs.(11) and (12) is disappeared.

$$\begin{aligned} w_0 &= W_0 \sin(m\pi x/a) \sin(n\pi y/b) \\ w &= W \sin(m\pi x/a) \sin(n\pi y/b) \end{aligned} \quad (13)$$

where, m is redefined and indicates the half-wave number matching with the buckling mode of the element, in which the subscript m attached in each coefficient was omitted.

The half-wave number m in Eq.(13) is dependent on the aspect ratio as well as the ratio of the biaxial loading components such that it may be altered if the loading ratio is changed in the subsequent loading step and then is determined as an integer that should be satisfied the following criterion [26-28].

$$\frac{(m^2 b^2/a^2 + 1)^2 / \{m^2 b^2/a^2 + \sigma_{yav}/\sigma_{xav}\}}{\leq \{(m+1)^2 b^2/a^2 + 1\}^2 / \{(m+1) b^2/a^2 + \sigma_{yav}/\sigma_{xav}\}} \quad (14)$$

By applying Galerkin method for the solving of the equilibrium and compatibility equation of the plate element, the following equation with regard to the unknown coefficient of the added deflection is emerged [6,27].

$$C_1 W^3 + C_2 W^2 + C_3 W + C_4 = 0 \quad (15)$$

where, $C_1 = E(m^4 \pi^2/a^4 + \pi^2/b^4)$

$$C_2 = 3W_0 C_1$$

$$C_3 = 2W_0^2 C_1 + 16\pi^2 D/t \{m^2/a^2 + 1/b^2\}^2 - 16\{m^2(\sigma_{xav} + \sigma_{rex})/a^2 + (\sigma_{yav} + \sigma_{rey})/b^2\}$$

$$C_4 = -16W_0 \{m^2(\sigma_{xav} + \sigma_{rex})/a^2 + (\sigma_{yav} + \sigma_{rey})/b^2\}$$

$$D = Et^3/12(1-\nu^2)$$

σ_{rex} and σ_{rey} in Eq.(15) indicates the effective compressive residual stresses of the plate element in x and y direction, respectively. If the actual compressive residual stresses in x and y direction that are present in the middle plate as shown in Fig.3 are denoted by σ_{rx} and σ_{ry} , respectively, then the effective compressive residual stresses are defined by [6,27]

$$\begin{aligned} \sigma_{rex} &= \sigma_{rx} \{1 - 0.5\sigma_{rx}/(\sigma_0 + \sigma_{rx})\} \\ \sigma_{rey} &= \sigma_{ry} \{1 - 0.5\sigma_{ry}/(\sigma_0 + \sigma_{ry})\} \end{aligned} \quad (16)$$

where, σ_0 indicates the yield stress of the material.

Eq.(15) is explicitly solved by using Cardano's method and if the unknown coefficient W is given, then membrane stress distribution of the element is precisely obtained. The maximum and minimum stresses are given by the following explicit form[6,27].

$$\begin{aligned} \sigma_{xmax} &= 0.5(\sigma_{xmax}^* - \sigma_{xmin}) \cos(2\pi\eta_x t/b) \\ &+ 0.5(\sigma_{xmax}^* + \sigma_{xmin}) \\ \sigma_{ymax} &= 0.5(\sigma_{ymax}^* - \sigma_{ymin}) \cos(2\pi\eta_y t/a) \\ &+ 0.5(\sigma_{ymax}^* + \sigma_{ymin}) \end{aligned} \quad (17)$$

$$\begin{aligned} \sigma_{xmin} &= \sigma_{xav} + \sigma_{rx} - \pi^2/8a^2 \cdot E \cdot W \cdot (W + 2W_0) \\ \sigma_{ymin} &= \sigma_{yav} + \sigma_{ry} - \pi^2/8b^2 \cdot E \cdot W \cdot (W + 2W_0) \end{aligned} \quad (18)$$

where, $\sigma_{xmax}^* = \sigma_{xav} + \pi^2/8a^2 \cdot E \cdot W \cdot (W + 2W_0)$
 $\sigma_{ymax}^* = \sigma_{yav} + \pi^2/8b^2 \cdot E \cdot W \cdot (W + 2W_0)$
 $\eta_x = \sigma_{rx} / (\sigma_0 + \sigma_{rx}) \cdot b/2t$
 $\eta_y = \sigma_{ry} / (\sigma_0 + \sigma_{ry}) \cdot a/2t$

where, subscript max and min denote the maximum and minimum stresses, respectively.

Substituting Eq.(17) into Eq.(8) and taking Eqs.(9) and (10) by the incremental form, the following relationship between average stress increment and average strain increment of the deflected plate element is emerged.

$$\{\Delta\sigma\} = [D]^E \{\Delta\epsilon\} \quad (19)$$

where, $\{\Delta\sigma\} = \{\Delta\sigma_{xav} \ \Delta\sigma_{yav} \ \Delta\tau_{xyav}\}^T$
 $\{\Delta\epsilon\} = \{\Delta\epsilon_{xav} \ \Delta\epsilon_{yav} \ \Delta\gamma_{xyav}\}^T$
 $[D]^E$ = the stress-strain matrix in the elastic range

$$= \begin{bmatrix} e_1 & e_2 & 0 \\ e_2 & e_3 & 0 \\ 0 & 0 & e_4 \end{bmatrix}^{-1}$$

$$\begin{aligned} e_1 &= (\partial\sigma_{xmax}/\partial\sigma_{xav})/E, \\ e_2 &= (\partial\sigma_{xmax}/\partial\sigma_{yav} - \nu)/E \\ &= (\partial\sigma_{ymax}/\partial\sigma_{xav} - \nu)/E \\ e_3 &= (\partial\sigma_{ymax}/\partial\sigma_{yav})/E, \\ e_4 &= 2(1+\nu)/E \end{aligned}$$

Thus, by using $[D]^E$ given in Eq.(19), the deflected plate element is replaced by the equivalent flat plate element which has zero deflection.

Tangential Elastic Stiffness Matrix. By applying the principle of the virtual work, the tangential elastic stiffness matrix of the plate element is derived. During the acting of the virtual displacement, the following equilibrium equation should be satisfied.

$$\delta\{AU\}^T \{R+AR\} = \int_V \delta\{\Delta\epsilon\}^T \{\sigma+\Delta\sigma\} dvol \quad (20)$$

The left hand side of the above equation indicates the work done by the external force and the right hand side is the strain energy stored in the element while the virtual

displacement is applied. Also, $\int_V(\cdot)dvol$ represents the integration for the entire volume of the element and prefix δ denotes the amount due to the virtual displacement. By making Eq.(6) a differentiation with respect to the displacement components, the virtual strain $\delta\{\Delta\epsilon\}$ shown in Eq.(20) is given by

$$\delta\{\Delta\epsilon\} = [B_p] \delta\{AU\} + [C+AC][G] \delta\{AU\} \quad (21)$$

By substituting Eqs.(19) and (21) into Eq.(20) and removing the unbalance force which is due to the discrepancy between the external force and the internal force, the tangential elastic stiffness equation of the deflected plate element is given by the following form.

$$\{AR\} = [K]^E \{AU\} \quad (22)$$

where, $[K]^E$ is the tangential elastic stiffness matrix of the element. Also, the tangential elastic stiffness matrix $[K]^E$ in Eq.(22) is given by applying updated Lagrangian approach.

$$\begin{aligned} [K]^E &= \int_V [B_p]^T [D]^E [B_p] dvol \\ &+ \int_V [G]^T [\sigma_b] [G] dvol \end{aligned} \quad (23)$$

where, $[\sigma_b] = \begin{bmatrix} \sigma_{xav} & \tau_{xyav} \\ \tau_{xyav} & \sigma_{yav} \end{bmatrix}$

$[D]^E$: the average stress-average strain matrix given in Eq.(19)

Displacement Function. In the present study, the plate behaviour is expressed by using three-degrees of freedom at each corner nodal point. Moreover since the equivalent flat plate element is employed instead of the deflected plate, the displacement function of in-plane as well as out-of-plane deformation takes the following linear form.

$$u = a_1 + a_2x + a_3y + a_4xy + b_4/2(b^2 - y^2) \quad (24.a)$$

$$v = b_1 + b_2x + b_3y + b_4xy + a_4/2(a^2 - x^2) \quad (24.b)$$

$$w = c_1 + c_2x + c_3y + c_4xy \quad (24.c)$$

where, coefficients a_1, a_2, \dots are the unknown constants which are expressed in terms of the nodal displacements. Also, Eqs.(24.a) and (24.b) indicate the in-plane displacement function, in which the last term at each right hand side is added such that the shearing strain inside the plate element remains uniform. Eq.(24.c) represents the out-of-plane displacement function. Accordingly, substituting Eq.(24) into Eq.(6) and performing the integration of Eq.(23) for the entire volume of the plate element, each component of the stiffness matrix will be obtained.

Ultimate Strength Criterion of the Element. With the increasing of the external load, the region where the stress level is high becomes to be yielded. As a result, the in-plane stiffness of the element decreases further and then the element reaches the ultimate limit state. The membrane stress

distribution of the deflected plate element is non-uniform and since the present plate element is dominantly subjected to biaxial load, the corner or the middle point of the edges in the longitudinal or transverse direction is likely to be yielded. If the corner where the maximum stress component is existed becomes to be yielded, then the plate element can not carry the further increasing of the external load. Also since the edges of the plate element remain straight, the tensile membrane stress may develop in the mid-edge of the plate depending on the loading ratio in the longitudinal and transverse direction. As long as the region where tensile stress acts is under elastic condition, the plate can resist against abrupt increase of the lateral deflection even though some portion inside of the element has already yielded. However, if the tensile part is yielded then the plate element collapses immediately. Therefore, the ultimate limit state of the plate element is judged whether or not the corner or the mid-edge becomes to be yielded in the present study. Accordingly, substituting the membrane stress components at each checking point into Mises's yielding condition, the following formula are emerged.

$$\begin{aligned} \Gamma_1 &= \sigma_{x\max}^2 - \sigma_{x\max} \cdot \sigma_{y\min} + \sigma_{y\min}^2 + 3\tau^2 - \sigma_0^2 \\ \Gamma_2 &= \sigma_{x\min}^2 - \sigma_{x\min} \cdot \sigma_{y\max} + \sigma_{y\max}^2 + 3\tau^2 - \sigma_0^2 \\ \Gamma_3 &= \sigma_{x\max}^2 - \sigma_{x\max} \cdot \sigma_{y\max} + \sigma_{y\max}^2 + 3\tau^2 - \sigma_0^2 \end{aligned} \quad (25)$$

where, $\sigma_{x\max}$, $\sigma_{y\max}$: Eq.(17)
 $\sigma_{x\min}$, $\sigma_{y\min}$: Eq.(18)
 $\tau (= \tau_{xyav})$: the average shearing stress

Also, index number indicates the plasticity checking point. Thus, if any one value of Γ given in Eq.(25) is equal to or greater than zero, then it is considered that the plate element has collapsed.

Post-Ultimate Stiffness Matrix. In the post-ultimate range of the element, the average internal stresses follow the unloading path even though the deformation increases continuously. In general, it is assumed that the magnitude of the stress components at the yielded point is not changed so seriously. Thus, when any one of plasticity checking point is yielded, that is, the element collapsed, the maximum membrane stress components at the yielded point are supposed to remain constant in the subsequent increasing of the deformation. Just after the element reaches the ultimate limit state, the membrane stress components at the yielded point are numerically given by

$$\begin{aligned} \sigma_{x\max}^u &= \sigma_{x\max}^u \\ \sigma_{y\max} &= \sigma_{y\max}^u \end{aligned} \quad (26)$$

where, superscript u indicates the value just after the element collapsed.

The average membrane stress components of the element in the post-ultimate range

are given by using the concept of the effective width[27].

$$\begin{aligned} \sigma_{xav} &= b_e/b \cdot \sigma_{x\max}^u \\ \sigma_{yav} &= a_e/a \cdot \sigma_{y\max}^u \end{aligned} \quad (27)$$

where, b_e and a_e represent the effective widths in the longitudinal and transverse direction, respectively.

With the increasing of the deformation, the effective widths continuously decrease even in the post-ultimate range. Here, the reduction tendency of the effective widths in the post-ultimate range is supposed to be same with the pre-ultimate range. Thus, the effective widths read

$$\begin{aligned} b_e/b &= \sigma_{xav}^* / \sigma_{x\max}^* \\ a_e/a &= \sigma_{yav}^* / \sigma_{y\max}^* \end{aligned} \quad (28)$$

where, σ_{xav}^* , σ_{yav}^* : the virtual average membrane stresses
 $\sigma_{x\max}^*$, $\sigma_{y\max}^*$: the virtual maximum membrane stresses

Also, the asterisk indicates that the stress is a virtual one in the post-ultimate range.

Since the large deformation has been occurred, the magnitude of the effective widths is considered to be very small such that the influence of the initial deflection is assumed to be not so serious in the post-ultimate range of the element[29]. For simplicity, therefore, the virtual average membrane stress is expressed in terms of the virtual maximum membrane stress that does not account for the influence of the initial deflection[28], that is,

$$\begin{aligned} \sigma_{xav}^* &= \frac{1}{a_1 b_x - a_2 b_1} [b_x \sigma_{x\max}^* - a_2 \sigma_{y\max}^* + a_2 b_1 - a_1 b_x] \\ \sigma_{yav}^* &= \frac{1}{a_1 b_x - a_2 b_1} [-b_1 \sigma_{x\max}^* + a_1 \sigma_{y\max}^* + a_2 b_1 - a_1 b_x] \end{aligned}$$

$$\text{where, } a_1 = 1 - \frac{2a^2}{a^4 + a^2/b^2}, \quad a_2 = -\frac{2a^2}{a^4/b^2 + a^2 + b^2}$$

$$b_1 = \frac{2a^2}{a^4/a^2 + a^2/b^2} \left(\frac{a^2}{c} - \frac{1}{b^2} \right)^2$$

$$b_2 = a_1, \quad b_2 = 1 - \frac{2}{a^2/b^2 + a^2 + 1}$$

$$b_3 = \frac{2}{a^4/b^2 + a^2 + 1/b^2} \left(\frac{a^2}{c} - \frac{1}{b^2} \right)^2 \quad (29)$$

Since the edges of the element remain straight, the virtual maximum membrane stresses are calculated by using the average strain as

$$\begin{aligned} \sigma_{x\max}^* &= E/(1-\nu^2) (\epsilon_{xav} + \nu \epsilon_{yav}) \\ \sigma_{y\max}^* &= E/(1-\nu^2) (\nu \epsilon_{xav} + \epsilon_{yav}) \end{aligned} \quad (30)$$

By substituting Eqs.(29) and (30) into Eq.(28), the effective widths in the post-ultimate range are expressed in terms of the average strain component. Also substituting the effective widths into Eq.(27), the average stress-average strain relation in the post-ultimate range is explicitly given, that is,

$$\begin{aligned} \sigma_{xav} &= \frac{\sigma_{max}^u}{E(a_1 b_2 - a_2 b_1)(\epsilon_x - \nu \epsilon_y)} [E(b_2 + \nu a_2) \epsilon_x - E(\nu b_2 + a_2) \epsilon_y + (1 - \nu^2)(a_2 b_3 - a_3 b_2)] \\ \sigma_{yav} &= \frac{\sigma_{max}^u}{E(a_1 b_2 - a_2 b_1)(\epsilon_y - \nu \epsilon_x)} [-E(b_1 + \nu a_1) \epsilon_x + E(\nu b_1 + a_1) \epsilon_y + (1 - \nu^2)(a_3 b_1 - a_1 b_3)] \end{aligned} \quad (31)$$

On the other hand, since the occurrence of the shear buckling is not expected in the present element, the shearing stiffness of the element is supposed to be fully effective even in the post-ultimate range. Thus, the same relation between the shearing stress and strain of Eq.(10) is employed. Taking Eqs.(31) and (10) by the incremental form, the following stress-strain relation in the post-ultimate range is emerged.

$$\{\Delta \sigma\} = [D]^u \{\Delta \epsilon\} \quad (32)$$

where, $[D]^u$ is the post-ultimate stress-strain matrix.

$$= \begin{bmatrix} d_1 & d_2 & 0 \\ d_2 & d_3 & 0 \\ 0 & 0 & d_4 \end{bmatrix}$$

$$\begin{aligned} d_1 &= \partial \sigma_{xav} / \partial \epsilon_{xav}, \quad d_2 = \partial \sigma_{xav} / \partial \epsilon_y \\ &= \partial \sigma_{yav} / \partial \epsilon_x, \quad d_3 = \partial \sigma_{yav} / \partial \epsilon_y, \\ d_4 &= E / 2(1 + \nu) \end{aligned}$$

Consequently, the post-ultimate stiffness matrix of the element is obtained by replacing $[D]^E$ in Eq.(23) with $[D]^u$ in Eq.(32). Thus,

$$[K]^u = \nu [B_p]^T [D]^u [B_p] dvol + \nu [G]^T [c_b] [G] dvol \quad (33)$$

where, $[K]^u$ is the post-ultimate stiffness matrix of the element.

CHARACTERISTICS OF THE PRESENT IDEALIZED PLATE ELEMENT

A computer program, ALPS/ISUM [22] is completed on the basis of the theory described in the previous section. Since the subject considered brings up a highly nonlinear problem, an incremental step-by-step procedure based on the updated Lagrangian approach is applied. The accuracy and efficiency of the program is verified comparing with the present solution and the existing experimental and numerical result for unit plate member and welded box-girder in this section.

Collapse Strength of Square Plates Under Uniaxial Compression

Ueda et.al. [30] conducted ultimate strength series tests for the welded square plates subjected to uniaxial compression. Table 1 represents the details of the specimen. Three kinds of plate thickness that are 4.5mm(A-specimen), 9.0mm(B-specimen) and 12.7mm(C-specimen) were tested. The boundary condition of the specimen in the experiment is set to be simply supported. The magnitude of the welding compressive residual stress for each specimen on which Ueda's measured

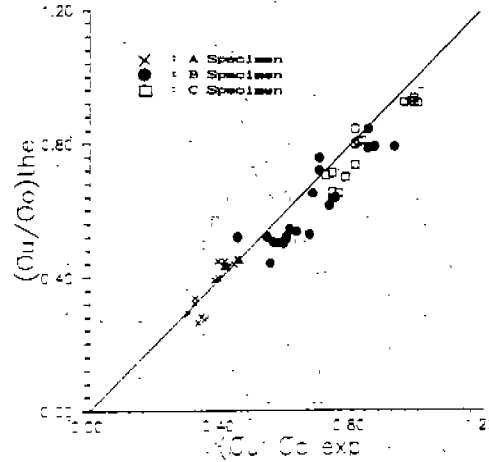


Fig.6 Comparison with the present solution and Ueda's experimental result for square plates under uniaxial compression

data is based is described in Table 1. Each specimen is modelled by using just one idealized plate element formulated in the present study and the total numbers of the nodal point and the degrees of freedom after the restraint condition is introduced are all four. A comparison between the experimental result and the present solution is made in Table 1 and Fig.6. It is clear that the present solution is in good agreement with Ueda's experimental results. Also since the computing time required in the present analysis was about 20 seconds by using IBM PC/AT computer, the present method is considered to be very efficient for the practical use.

Collapse Strength of Rectangular Plates Under Uniaxial Compression

In order to investigate the influence of the aspect ratio on the ultimate strength of the plate element, elasto-plastic large deflection analysis of initially deflected rectangular plates is performed by applying the nonlinear finite element method developed by the author[31]. These results are then compared with the solution obtained by the present method. Table 2 indicates the dimensions of the plates. The maximum magnitude of the initial deflection is set to be 10 percent of the plate thickness. The shape of the initial deflection of the rectangular plates was assumed as shown in Fig.4.b. The configuration of the initial deflection is depicted by Fourier series function using 15 terms. As mentioned earlier, the present theory selects only the buckling mode component as the deflection

Table 1. Description of Ueda's test specimen for the welded square plate subjected to uniaxial compression

| Specimen No. | t (mm) | σ_0 (kg/mm ²) | b/t | W ₀ /t | σ_{rx} (kg/mm ²) | E X P. | | T H E. | |
|--------------|--------|----------------------------------|--------|-------------------|-------------------------------------|------------|---------------------|------------|---------------------|
| | | | | | | σ_u | σ_u/σ_0 | σ_u | σ_u/σ_0 |
| A-1 | 4.50 | 28.48 | 111.11 | 0.00 | 2.00 | 11.11 | 0.39 | 12.79 | 0.45 |
| A-2 | 4.50 | 26.59 | 111.11 | 0.00 | 2.00 | 11.96 | 0.45 | 12.10 | 0.46 |
| A-3 | 4.50 | 26.66 | 111.11 | 0.09 | 2.00 | 10.93 | 0.41 | 11.94 | 0.45 |
| A-4 | 4.50 | 26.00 | 111.11 | 0.09 | 2.00 | 11.96 | 0.46 | 11.67 | 0.45 |
| A-5 | 4.50 | 25.87 | 111.11 | 0.09 | 2.00 | 11.64 | 0.45 | 11.67 | 0.45 |
| A-6 | 4.50 | 26.27 | 111.11 | 0.24 | 2.00 | 11.56 | 0.44 | 11.51 | 0.44 |
| A-7 | 4.50 | 28.07 | 111.11 | 0.27 | 2.00 | 11.51 | 0.41 | 12.15 | 0.43 |
| A-8 | 4.50 | 26.45 | 111.11 | 0.31 | 2.00 | 11.11 | 0.42 | 11.43 | 0.43 |
| A-9 | 4.50 | 26.88 | 111.11 | 0.36 | 2.00 | 11.29 | 0.42 | 11.56 | 0.43 |
| A-10 | 4.50 | 26.66 | 111.11 | 0.38 | 2.00 | 10.93 | 0.41 | 11.46 | 0.43 |
| A-11 | 4.50 | 28.03 | 111.11 | 0.89 | 2.00 | 10.93 | 0.39 | 11.18 | 0.40 |
| A-12 | 4.50 | 25.16 | 111.11 | 1.02 | 2.00 | 9.56 | 0.38 | 9.84 | 0.39 |
| A-13 | 4.34 | 22.01 | 115.21 | 0.33 | 5.00 | 6.98 | 0.32 | 7.40 | 0.34 |
| A-14 | 4.34 | 22.01 | 115.21 | 0.52 | 5.00 | 7.12 | 0.32 | 7.09 | 0.32 |
| A-15 | 4.34 | 23.42 | 115.21 | 1.07 | 5.00 | 7.05 | 0.30 | 6.84 | 0.29 |
| A-16 | 4.34 | 23.08 | 115.21 | 1.28 | 5.00 | 7.81 | 0.34 | 6.49 | 0.28 |
| A-17 | 4.34 | 21.05 | 115.21 | 1.31 | 5.00 | 7.28 | 0.35 | 5.75 | 0.27 |
| A-18 | 4.34 | 22.87 | 115.21 | 1.74 | 5.00 | 7.66 | 0.33 | 6.01 | 0.26 |
| B-1 | 8.80 | 31.03 | 56.82 | 0.00 | 2.00 | 27.00 | 0.87 | 24.48 | 0.79 |
| B-2 | 8.80 | 31.20 | 56.82 | 0.00 | 2.00 | 26.52 | 0.85 | 24.46 | 0.78 |
| B-3 | 8.80 | 31.06 | 56.82 | 0.00 | 2.00 | 28.89 | 0.93 | 24.48 | 0.79 |
| B-4 | 9.00 | 28.71 | 55.56 | 0.00 | 2.00 | 24.40 | 0.85 | 24.12 | 0.84 |
| B-5 | 8.80 | 31.96 | 56.82 | 0.26 | 2.00 | 21.73 | 0.68 | 20.74 | 0.65 |
| B-6 | 8.80 | 31.27 | 56.82 | 0.31 | 2.00 | 23.14 | 0.74 | 19.83 | 0.63 |
| B-7 | 8.80 | 30.91 | 56.82 | 0.31 | 2.00 | 23.18 | 0.75 | 19.66 | 0.64 |
| B-8 | 8.80 | 30.21 | 56.82 | 0.38 | 2.00 | 20.05 | 0.73 | 18.52 | 0.61 |
| B-9 | 8.80 | 32.11 | 56.82 | 0.61 | 2.00 | 19.59 | 0.61 | 17.44 | 0.54 |
| B-10 | 9.00 | 28.63 | 55.56 | 0.68 | 2.00 | 18.04 | 0.63 | 15.32 | 0.54 |
| B-11 | 9.00 | 25.07 | 55.56 | 0.72 | 2.00 | 16.80 | 0.67 | 13.21 | 0.53 |
| B-12 | 8.80 | 30.53 | 56.82 | 0.73 | 2.00 | 18.32 | 0.60 | 15.68 | 0.52 |
| B-13 | 8.80 | 30.30 | 56.82 | 0.75 | 2.00 | 18.18 | 0.60 | 15.60 | 0.52 |
| B-14 | 8.80 | 30.52 | 56.82 | 0.82 | 2.00 | 17.70 | 0.58 | 15.32 | 0.50 |
| B-15 | 9.00 | 25.39 | 55.56 | 0.84 | 2.00 | 14.98 | 0.59 | 12.70 | 0.50 |
| B-16 | 8.85 | 25.60 | 56.50 | 0.02 | 5.00 | 18.03 | 0.70 | 19.38 | 0.76 |
| B-17 | 8.95 | 26.81 | 55.87 | 0.06 | 5.00 | 18.91 | 0.70 | 19.25 | 0.72 |
| B-18 | 8.83 | 25.28 | 56.63 | 0.48 | 5.00 | 13.55 | 0.54 | 13.15 | 0.52 |
| B-19 | 8.70 | 25.55 | 57.47 | 0.49 | 5.00 | 14.34 | 0.56 | 12.85 | 0.50 |
| B-20 | 8.80 | 25.55 | 56.82 | 0.71 | 5.00 | 14.05 | 0.55 | 11.27 | 0.44 |
| B-21 | 8.70 | 25.55 | 57.47 | 0.77 | 5.00 | 11.49 | 0.45 | 13.29 | 0.52 |
| C-1 | 12.80 | 25.20 | 39.06 | 0.00 | 2.00 | 24.19 | 0.96 | 23.21 | 0.92 |
| C-2 | 12.80 | 25.09 | 39.06 | 0.00 | 2.00 | 24.84 | 0.99 | 23.13 | 0.92 |
| C-3 | 12.80 | 25.09 | 39.06 | 0.00 | 2.00 | 24.59 | 0.98 | 23.13 | 0.92 |
| C-4 | 12.80 | 25.03 | 39.06 | 0.00 | 2.00 | 25.03 | 1.00 | 23.00 | 0.92 |
| C-5 | 12.90 | 30.16 | 38.76 | 0.00 | 2.00 | 29.86 | 0.99 | 28.14 | 0.93 |
| C-6 | 13.30 | 29.52 | 37.59 | 0.20 | 2.00 | 23.91 | 0.81 | 24.86 | 0.84 |
| C-7 | 13.30 | 29.51 | 37.59 | 0.20 | 2.00 | 24.50 | 0.83 | 23.81 | 0.81 |
| C-8 | 12.90 | 30.46 | 38.76 | 0.25 | 2.00 | 24.67 | 0.81 | 24.25 | 0.80 |
| C-9 | 13.30 | 29.34 | 37.59 | 0.26 | 2.00 | 24.06 | 0.82 | 23.56 | 0.80 |
| C-10 | 12.91 | 30.32 | 38.76 | 0.36 | 2.00 | 24.56 | 0.81 | 22.25 | 0.73 |
| C-11 | 13.30 | 29.47 | 37.59 | 0.42 | 2.00 | 21.80 | 0.74 | 20.95 | 0.71 |
| C-12 | 12.90 | 30.49 | 38.76 | 0.43 | 2.00 | 23.78 | 0.78 | 21.25 | 0.70 |
| C-13 | 13.30 | 29.32 | 37.59 | 0.43 | 2.00 | 21.11 | 0.72 | 20.61 | 0.70 |
| C-14 | 12.90 | 30.15 | 38.76 | 0.52 | 2.00 | 22.31 | 0.74 | 19.89 | 0.65 |
| C-15 | 12.90 | 30.29 | 38.76 | 0.53 | 2.00 | 23.02 | 0.76 | 19.69 | 0.65 |

Table 2 Description of the rectangular plates subjected to uniaxial compression

| a/b | b (mm) | t (mm) | σ_0 (kg/mm ²) | σ_u (kg/mm ²) | | | Mesh Size in FEM Ana. | W_{in} | CPU Time by CYBER 932/31 for FEM Ana. (Min.) |
|-----|--------|--------|----------------------------------|----------------------------------|--------------|---------|-----------------------|----------|----------------------------------------------|
| | | | | FEM | FEM (10% Up) | Present | | | |
| 1 | 500 | 10 | 36 | 27.48 | 30.23 | 29.21 | 5 x 5 | 1.0000 | 23.0 |
| 2 | 500 | 10 | 36 | 30.90 | 33.99 | 32.57 | 10 x 5 | 0.0000 | 45.3 |
| 3 | 500 | 10 | 36 | 28.80 | 31.68 | 31.41 | 15 x 5 | 0.3335 | 72.4 |
| 4 | 500 | 10 | 36 | 29.40 | 32.34 | 32.61 | 20 x 5 | 0.0000 | 103.5 |
| 5 | 500 | 10 | 36 | 29.06 | 31.97 | 32.04 | 25 x 5 | 0.2014 | 141.1 |

Note : 1) Mesh size in FEM analysis indicates meshes for a quarter plate in the longitudinal and transverse direction
 2) W_{in} denotes the magnitude of initial deflection for buckling wave number

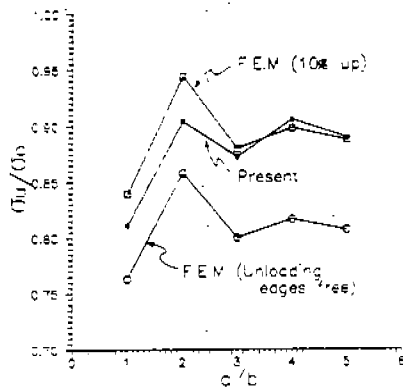


Fig. 7 Comparison with the present solution and FEM result for rectangular plates under uniaxial compression

parameter. Table 2 gives the buckling mode component of the initial deflection for each plate. The yield stress of the material is assumed to be 36 kg/mm² and Young's modulus is 21000 kg/mm². The welding residual stress is not present. In FE analysis, due to the geometric symmetry, a quarter of the plate is modelled. The mesh size number varying aspect ratio is given in Table 2, in which the rectangular plate element having four corner nodal points is employed. Since the unloading edges of the specimen have no restraints to the in-plane movement, it is expected that the ultimate strength is underestimated by about 10 percent less than the case that the edges remain straight. Thus, Table 2 also compares with the present solution and the corrected ultimate strength by adding up 10 percent, because the idealized plate element was formulated under the consideration that the edges remain straight. Table 2 gives the comparison between the solutions by FEM and present method. Fig. 7 shows the change of the ultimate strength with varying the aspect ratio of the plate. Accuracy of the present solution is sufficient comparing with FEM result. The computing times required in FE analysis by using CYBER 932/31 computer are given in Table 2, while the present analysis needed only 20 seconds by IBM PC/AT computer. It is obvious that the present method is very efficient.

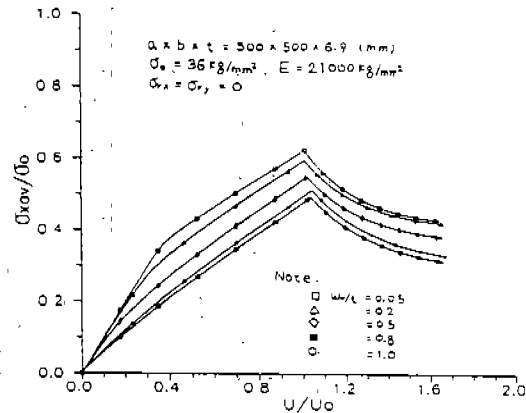


Fig. 8 The load-displacement behaviour of a square plate under uniaxial displacement obtained by the present method with varying the magnitude of the initial deflection

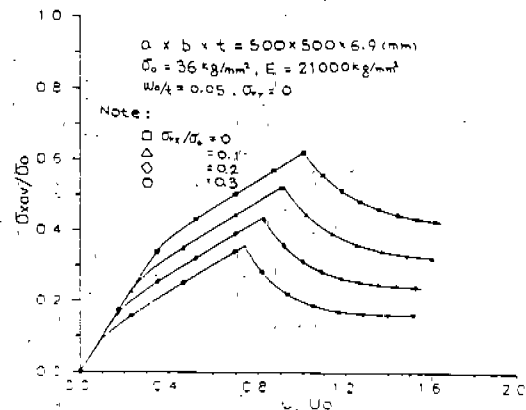


Fig. 9 The load-displacement behaviour of a square plate under uniaxial displacement obtained by the present method with varying the magnitude of the residual stress

Post-Ultimate Behaviour of Square Plate Under Uniaxial Compression

In order to demonstrate the applicability of the present theory in the post-ultimate range, post-ultimate behaviour of simply supported square plates subjected to uniaxial compression is analyzed. Fig.8 and 9 represent the load-shortening curve for an imperfect square plate subjected to uniaxial displacement. Here, Fig.8 and 9 are results obtained with varying the magnitude of the initial deflection and welding residual stress, respectively. It is clear that the present method gives a reasonable solution even in the post-ultimate range of the element.

Collapse Strength of Welded Box-Column

Usami et.al. [32] conducted ultimate strength series tests for welded box-columns in order to investigate the interaction effect between local and overall buckling of the structure. Fig.10 shows the configuration of the specimen and their detail dimensions are given in Table 3. Among these, S-series indicates that the shape of box section of the specimen is nearly square, while R-series represents the specimen having the rectangular shape of the section. Also, shorter specimen such as S-10 and R-10 series has only end-diaphragms which are installed in both ends of the structure but longer specimen has two more inside-diaphragms in addition to end-diaphragms as shown in Fig.10. The box columns are composed of thin plate elements and each plate element is modelled by an idealized plate element. Here, diaphragm is also modelled by an idealized plate element. As shown in Fig.10, the end-diaphragm is located slightly inside from both ends and for the simplicity of the modelling the plate fragments outside of the end-diaphragm is neglected in the present analysis. The boundary and loading condition are shown in Fig.10. The loading is incrementally applied by a displacement control. A comparison between the ultimate strength obtained by experiment and present analysis is made in Table 3 and Fig.11. It is observed that the present solution is in good agreement with the experimental result. The computing time required in the present analysis was about 30 seconds for shorter column and 5 minutes for longer column by using CYBER 932/31 computer.

APPLICATION OF THE PRESENT METHOD TO OBJECTIVE DOUBLE SKIN HULL GIRDER

Structural Modelling

Fig.12 shows a structural modelling using the idealized plate element. A half length of one cargo hold located at midship is chosen as the extent of the analysis. Also because of the symmetry with regard to the center line, a half breadth of the hull girder is modelled. Fig.13 represents outline of the boundary and loading condition. The longitudinal displacement along the left-end

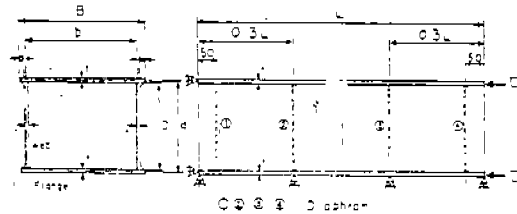


Fig.10 Usami's test set-up for welded box-column

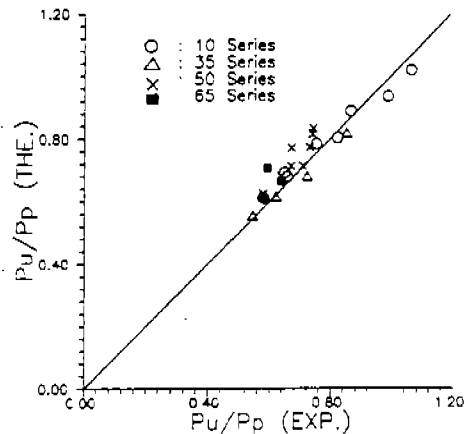


Fig.11 Comparison with present solution and Usami's experimental result for welded box-column

of the hold is restrained. The symmetric condition is introduced at the center line. The bottom at the loading position is fixed toward the depth direction. The vertical bending moment is generated by the displacement control with respect to the neutral axis such that the cross-section of the hull at the loading position keeps plane state. The neutral axis is positioned at 13.816 m above the bottom keel as shown in Fig.1. Because of the action of the vertical bending moment, if the upper deck panel or bottom plating that is subjected to axial compression is yielded in the earlier stage than the side shell plating, the position of the neutral axis is expected to be moved toward the opposite part that is under the tensile loading. As a result, the side shell plating contributes to sustain the further increasing of the external load instead of the failed deck or bottom substructure and then a slight increase of the calculated load carrying capacity is expected. According to the research result of Ref.[33], however, the influence of the change of neutral axis position on the ultimate longitudinal strength of the hull girder is not so serious and thus for simplicity the present study postulates that the position of the neutral axis is not changed even after local failures are occurred, which results in the slight underestimation of the ultimate longitudinal strength of the hull girder. The total numbers of idealized plate elements and nodal points employed in the present analysis are

Table 3 Description of Usami's test specimen for the welded box column

| Specimen No. | B (mm) | D (mm) | t (mm) | L (mm) | E X P. | | T H E. | |
|--------------|--------|--------|--------|--------|-------------|-----------|-------------|-----------|
| | | | | | P_u (ton) | P_u/P_p | P_u (ton) | P_u/P_p |
| S-10-22 | 151 | 127 | 6.01 | 501 | 249.5 | 0.987 | 235.5 | 0.932 |
| S-10-27 | 181 | 156 | 6.00 | 650 | 264.5 | 0.865 | 270.8 | 0.886 |
| S-10-33 | 217 | 183 | 6.00 | 800 | 280.5 | 0.753 | 291.7 | 0.783 |
| S-10-38 | 246 | 223 | 6.00 | 900 | 280.0 | 0.657 | 289.3 | 0.679 |
| S-10-44 | 283 | 259 | 6.03 | 1000 | 287.0 | 0.579 | 303.5 | 0.612 |
| R-10-22 | 151 | 93.5 | 5.98 | 500 | 235.0 | 1.063 | 203.1 | 0.919 |
| | | | | | | | 224.6* | 1.016* |
| R-10-33 | 217 | 144 | 6.00 | 700 | 269.5 | 0.822 | 283.1 | 0.802 |
| R-10-44 | 283 | 193 | 6.05 | 900 | 283.0 | 0.649 | 319.7 | 0.733 |
| | | | | | | | 301.8* | 0.692* |
| S-35-22 | 151 | 127 | 6.00 | 1880 | 215.5 | 0.852 | 206.5 | 0.816 |
| S-35-27 | 182 | 157 | 6.02 | 2310 | - | - | 238.1 | |
| S-35-33 | 216 | 193 | 6.03 | 2830 | 269.5 | 0.722 | 254.0 | 0.680 |
| S-35-38 | 247 | 223 | 6.01 | 3280 | 265.5 | 0.621 | 282.8 | 0.615 |
| S-35-44 | 283 | 259 | 6.01 | 3770 | 268.5 | 0.544 | 273.9 | 0.555 |
| S-50-22 | 151 | 122 | 6.01 | 2690 | 183.5 | 0.740 | 201.9 | 0.814 |
| S-50-27 | 181 | 157 | 6.00 | 3300 | 206.5 | 0.672 | 236.9 | 0.771 |
| S-50-33 | 217 | 192 | 6.00 | 4040 | 249.0 | 0.670 | 284.8 | 0.712 |
| R-50-22 | 151 | 94.2 | 6.00 | 2090 | 165.5 | 0.743 | 185.4 | 0.832 |
| R-50-27 | 181 | 116 | 6.00 | 2570 | 197.0 | 0.731 | 207.8 | 0.772 |
| R-50-33 | 217 | 144 | 6.00 | 3140 | 232.5 | 0.709 | 233.4 | 0.712 |
| R-50-38 | 247 | 166 | 6.00 | 3610 | 240.0 | 0.639 | 255.1 | 0.679 |
| R-50-44 | 283 | 193 | 6.01 | 4180 | 250.5 | 0.579 | 270.2 | 0.624 |
| R-65-22 | 151 | 94.4 | 6.01 | 2720 | 132.5 | 0.593 | 185.5 | 0.830 |
| | | | | | | | 157.8** | 0.706** |
| R-65-27 | 181 | 116 | 6.00 | 3340 | 171.5 | 0.637 | 211.5 | 0.785 |
| | | | | | | | 178.8** | 0.664** |
| R-65-33 | 217 | 143 | 6.00 | 4080 | 181.5 | 0.585 | 236.5 | 0.722 |
| | | | | | | | 198.1** | 0.605** |

- Note: 1) P_u and P_p denote the ultimate strength and fully plastic strength, respectively
- 2) Symbols "S" and "R" in specimen number indicate that the shapes of the box section are square and rectangular, respectively
 - 3) Values of initial imperfections measured for typical specimen are $\sigma_r/\sigma_0 = 0.087-0.136$ (average=0.112) and $\delta_0/L = 0.31-6.29(x10^{-4})$
 - 4) Assumed values of initial imperfections used in the present analysis are $\sigma_r/\sigma_0 = 0.112$, $\delta_0/L = 6.29x10^{-4}$ and $w_0/t = 0.1$
 - 5) Values marked by asterisk(*) were calculated under consideration of no residual stress and no initial deflection
 - 6) Values marked by asterisk(**) were obtained under the consideration of $\sigma_r/\sigma_0 = 0.2$, $\delta_0/L = 6.29x10^{-4}$ and $w_0/t = 0.3$

116 and 162, respectively. Series analysis of 20 cases denoted in Table 4 was performed varying the magnitude of the initial deflection and welding residual stress. S and H series denote the sagging and hogging condition, respectively. For simplicity, all plate elements are supposed to have the same ratio of the initial imperfections such as w_0/t and σ_{rx}/σ_0 . Two kinds of shape of the initial deflection shown in Fig.4 are considered. The compressive residual stress in the transverse direction of the hull girder is set to be zero in the present analysis. For each calculation, about only 7 minutes were required by using MIPS-M/120 super mini-computer.

Numerical Results and Discussions

First, in order to investigate the nonlinear behaviour of the hull girder with the increasing the vertical bending moment,

the result of SA and HA case are observed. Fig.14 represents the vertical bending moment-rotation curve of the hull girder. According to the sagging or hogging condition, the deck panel or bottom plating failed first. As a result, the overall bending stiffness of the hull girder was progressively decreased. After the longitudinal girder in deck panel or bottom plating failed, finally the hull girder collapsed as a whole.

Next, the influence of the initial deflection on the ultimate longitudinal strength is investigated. As described in Fig.4, two kinds of shape of the initial deflection are considered. Fig.15.a and 15.b are results obtained for the shape of the initial deflection of Fig.4.a and 4.b, respectively. According to these results, when the initial deflection of the plate element has the shape of Fig.4.a that matches

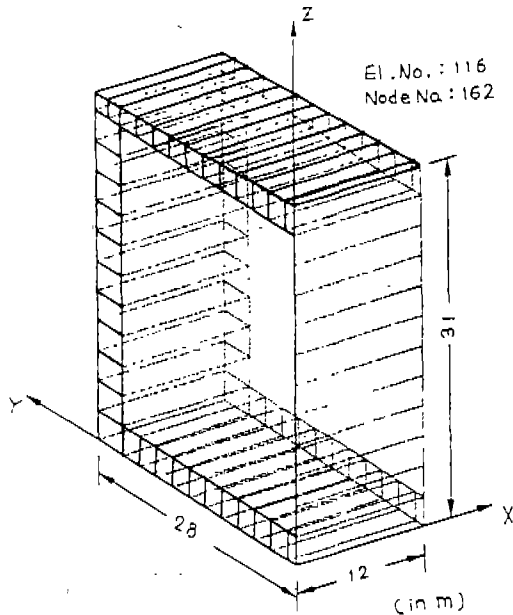


Fig.12 Structural modelling by using the idealized plate element

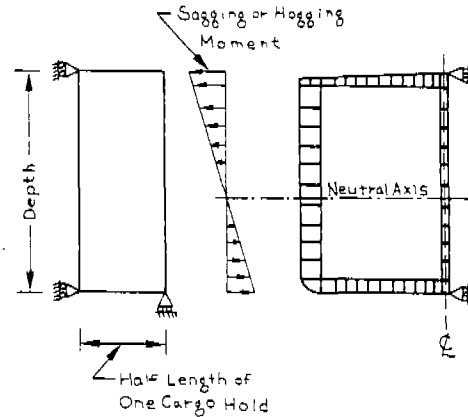


Fig.13 Outline of the loading and boundary condition

Table 4 Description of the parametric analysis for the ultimate longitudinal strength of the hull girder

| Case No. | Load Cond. | W ₀ /t | σ_{rx}/σ_0 | σ_{ry}/σ_0 | Shape of Initial Deflection |
|----------|------------|-------------------|------------------------|------------------------|-----------------------------|
| SA | Sag. | 0.05 | 0.0 | 0.0 | |
| SB | - | 0.2 | - | - | " |
| SC | - | 0.5 | - | - | " |
| SD | - | 1.0 | - | - | " |
| SE | - | 0.05 | - | - | |
| SF | - | 0.2 | - | - | " |
| SG | - | 0.5 | - | - | " |
| SH | - | 1.0 | - | - | " |
| SI | - | 0.05 | 0.1 | - | |
| SJ | - | - | 0.2 | - | " |
| HA | Hog. | 0.05 | 0.0 | 0.0 | |
| HB | - | 0.2 | - | - | " |
| HC | - | 0.5 | - | - | " |
| HD | - | 1.0 | - | - | " |
| HE | - | 0.05 | - | - | |
| HF | - | 0.2 | - | - | " |
| HG | - | 0.5 | - | - | " |
| HH | - | 1.0 | - | - | " |
| HI | - | 0.05 | 0.1 | - | |
| HJ | - | - | 0.2 | - | " |

the buckling mode of the plate, the initial deflection reduces the ultimate longitudinal strength of the hull girder. However, the shape of Fig.4.b gives rise to opposite or no effect on the ultimate longitudinal strength. This phenomenon is due that if the shape of the initial deflection is not same as buckling mode, the initial deflection increases the ultimate compressive strength of the plate[34-36]. Fig.16 indicates the vertical bending moment-rotation curve with varying the magnitude of the compressive residual stress which is existed in the

longitudinal direction of the hull girder. It is observed that because of the existence of the compressive residual stress the ultimate longitudinal strength of the hull girder is seriously reduced. The assessment result of the reserve strength factor and the safety index is given in Table 5. It is observed that the present double skin hull girder has sufficient safety in the longitudinal strength point of view because reserve strength factor and safety index are considered to be relatively large.

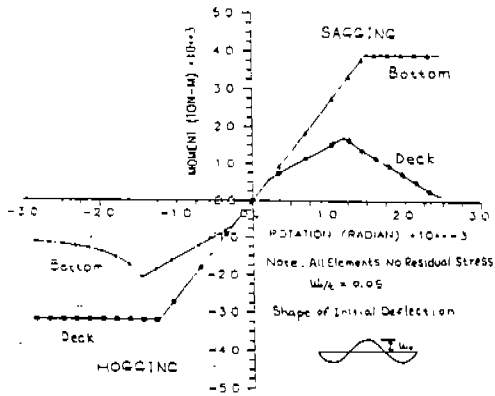


Fig. 14 The vertical bending moment-rotation curve for SA and HA case

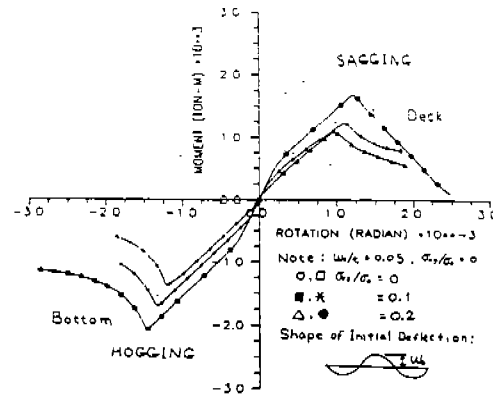


Fig. 16 The vertical bending moment-rotation curve of the hull girder varying the magnitude of the residual stress

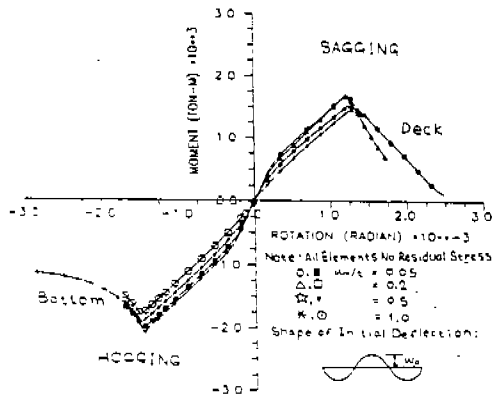


Fig. 15.a The vertical bending moment-rotation curve of the hull girder varying the magnitude of initial deflection with buckling mode shape

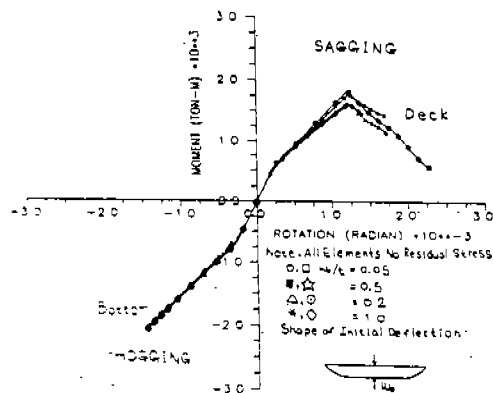


Fig. 15.b The vertical bending moment-rotation curve of the hull girder varying the magnitude of initial deflection with the shape of hungry horse's back

CONCLUDING REMARKS AND FUTURE RESEARCH WORK

In order to make a system safety assessment of ship's hull girder in the longitudinal strength point of view, evaluation of ultimate longitudinal bending strength is one of key issues. Also structural designers are necessary to have detail understanding of progressive collapse history as well as ultimate collapse capacity such that they can determine the structural layouts more reasonably and efficiently. In this study, an attempt is made such that the progressive collapse strength of ship's hull girder under sagging or hogging bending moment is efficiently analyzed by using idealized structural unit method. An idealized plate element subjected to biaxial load is formulated taking account of the influence of the initial imperfections as well as the interaction effect between the local and overall buckling in the structure. A computer program, ALPS/ISUM is completed based on the present theory and the accuracy and efficiency of the present method are verified through comparing the present solution with the existing experimental and numerical result. The present method is then applied to the ultimate longitudinal strength analysis of 280K double skin tanker as a simple example. A parametric analysis with varying the initial deflection and welding residual stress is performed. Based on the results obtained here, assessment of the reserve strength factor and safety index is made. It is observed that the initial imperfections existing in the local plate element reduce system safety of ship's hull girder and the double skin hull girder designed in this study has sufficient safety in the longitudinal strength point of view.

Although the example hull structure designed in this study is at present somewhat unrealistic type of the double skin tanker, it is found from the results of this study that the present method can be applied to the nonlinear analysis of large size plated

Table 5 Safety assessment result for the example hull girder

| Case No. | \bar{M}_s (ton-m) | \bar{M}_w (ton-m) | \bar{M}_v (ton-m) | γ | β |
|----------|------------------------|------------------------|------------------------|----------|---------|
| SA | 1692.4 | 438.2 | 642.9 | 1.565 | 2.817 |
| SB | 1680.1 | - | - | 1.554 | 2.772 |
| SC | 1508.4 | - | - | 1.395 | 2.105 |
| SD | 1436.5 | - | - | 1.331 | 1.806 |
| SE | 1817.9 | - | - | 1.682 | 3.247 |
| SF | 1626.6 | - | - | 1.505 | 2.574 |
| SG | 1756.8 | - | - | 1.625 | 3.043 |
| SH | 1589.8 | - | - | 1.471 | 2.433 |
| SI | 1241.4 | - | - | 1.148 | 0.871 |
| SJ | 1088.2 | - | - | 1.007 | 0.041 |
| HA | 2087.8 | - | - | 1.931 | 4.042 |
| HB | 2018.4 | - | - | 1.867 | 3.853 |
| HC | 1922.5 | - | - | 1.778 | 3.574 |
| HD | 1796.1 | - | - | 1.629 | 3.175 |
| HE | 2112.0 | - | - | 1.954 | 4.105 |
| HF | 2105.0 | - | - | 1.947 | 4.087 |
| HG | 2091.3 | - | - | 1.934 | 4.051 |
| HH | 2073.1 | - | - | 1.918 | 4.002 |
| HI | 1704.3 | - | - | 1.576 | 2.859 |
| HJ | 1381.1 | - | - | 1.277 | 1.549 |

- Note : 1) γ and β denote the reserve strength factor and safety index, respectively
 2) \bar{M}_s , \bar{M}_w and \bar{M}_v indicate mean value of the ultimate, still water and wave-induced vertical bending moment, respectively
 3) COVs of \bar{M}_s , \bar{M}_w and \bar{M}_v are assumed to be 10%, 10% and 20%, respectively

structure such as the double skin hull girder because the computing time required is very small while giving a reasonable result. Thus, it will be useful when ultimate collapse strength-based safety assessment or optimization is made in the structural design stage for a new type of hull girder. However, since the ship's hull girder is usually composed of stiffened plate element, the idealized stiffened plate element should be developed in order to carry out the nonlinear analysis for more realistic type of hull structure. Also in general, because the unstiffened and stiffened plate element are subjected to shearing force and lateral load as well as biaxial loads, the influence of the other loading components on the behaviour of plate element itself should be incorporated into each idealized structural element.

ACKNOWLEDGEMENT

The present study was conducted under the financial support of Korea Science and Engineering Foundation (Project No.: KOSEF - 89-0206-04).

REFERENCES

1. T. Okamoto et al., "Strength Evaluation of Novel Unidirectional-Girder System Product Oil Carrier by Reliability Analysis", *Trans. SNAME*, 1985.

2. RINA, "New-Generation Supertankers Above 100,000 DWT", *The Naval Architect*, Sep., 1990.
3. E. Nikolaidis and K. Kapania, "System Reliability and Redundancy of Marine Structures : A Review of the State of the Art", *J. of Ship Research*, Vol. 34, No. 1, 1990.
4. Y. Ueda and S. M. H. Rashed, "An Ultimate Transverse Strength Analysis of Ship Structures", *J. of Society of Naval Architects of Japan*, Vol. 136, 1974 (in Japanese).
5. Y. Ueda and S. M. H. Rashed, "The Idealized Structural Unit Method and Its Application to Deep Girder Structures", *Computers & Structures*, Vol. 18, 1984.
6. Y. Ueda, S. M. H. Rashed and J. K. Paik, "Plate and Stiffened Plate Units of the Idealized Structural Unit Method (1st Report)", *J. of Society of Naval Architects of Japan*, Vol. 156, 1984 (in Japanese).
7. Y. Ueda, S. M. H. Rashed and J. K. Paik, "Plate and Stiffened Plate Units of the Idealized Structural Unit Method (2nd Report)", *J. of Society of Naval Architects of Japan*, Vol. 159, 1986 (in Japanese).

8. Y.Ueda, S.M.H.Rashed and M.Katayama, "Ultimate Strength Analysis of Double Bottom Structures by Idealized Structural Unit Method", J. of Society of Naval Architects of Japan, Vol.138, 1975 (in Japanese).
9. Y.Ueda et.al., "Ultimate Strength Analysis of Double Bottom Structures in Stranding Conditions", Proc. of 3rd International Symposium on Practical Design of Ships and Mobile Units, Trondheim, Norway, 1987.
10. J.K.Paik et.al., "Damage and Strength Analysis of Double Bottom Structures in Stranding", Proc. of the Autumn Meeting of Society of Naval Architects of Korea, 1990 (in Korean).
11. J.K.Paik, "Ultimate Strength Analysis of Ship Structures by Idealized Structural Unit Method", Dr. Dissertation, Osaka University, Japan, 1987 (in Japanese).
12. J.K.Paik, "Ultimate Longitudinal Strength Analysis of the Double Skin Tanker by Idealized Structural Unit Method", Proc. of the Autumn Meeting of Society of Naval Architects of Korea, 1990 (in Korean).
13. J.K.Paik and D.H.Lee, "Ultimate Longitudinal Strength-Based Safety and Reliability Assessment of Ship's Hull Girder", J. of Society of Naval Architects of Japan, Vol.168, 1990.
14. S.M.H.Rashed, "Ultimate Strength and Post-Ultimate Strength Behaviour of Damaged Tubular Structural Members", Division of Marine Structures, Norwegian Institute of Technology, Report No. SK/R52, 1980.
15. Y.Ueda and S.M.H.Rashed, "Behaviour of Damaged Tubular Structural Members", J. of Energy Resources Technology, ASME, Vol.107, 1985.
16. Y.Ueda, S.M.H.Rashed and K.Nakacho, "New Efficient and Accurate Method of Nonlinear Analysis of Offshore Frames(The Idealized Structural Unit Method)", J. of Energy Resources Technology, ASME, Vol.107, 1985.
17. S.M.H.Rashed et.al., "Ultimate Strength of Jack-Up Rigs in Survival and Punch-Through Conditions", Proc. of 3rd International Symposium on Practical Design of Ships and Mobile Units, Trondheim, Norway, 1987.
18. T.Yao, J.Taby and T.Moan, "Ultimate Strength and Post-Ultimate Strength Behaviour of Damaged Tubular Members in Offshore Structures", J. of Offshore Mechanics and Arctic Engineering, ASME, Vol.110, 1988.
19. J.K.Paik and B.C.Shin, "Theoretical and Experimental Study for the Progressive Collapse Strength Analysis of Tubular Offshore Structures", Proc. of 1st Pacific/Asia Offshore Mechanics Symposium, Seoul, Korea, 1990.
20. J.K.Paik and H.K.Lim, "A Study on the Ultimate Strength Analysis of Frame Structures by Idealized Structural Unit Method", Proc. of the Autumn Meeting of Computational Structural Engineering Institute of Korea, 1990.
21. J.K.Paik and H.K.Lim, "Progressive Collapse Strength Analysis of Jacket Type Offshore Structure", Proc. of the Autumn Meeting of Korea Committee for Ocean Resources & Engineering, 1990 (in Korean).
22. J.K.Paik, ALPS/ISUM User's Manual (Version 6.5), A Computer Program for Analysis of Large Plated Structure by Idealized Structural Unit Method, Department of Naval Architecture, Pusan National University, Report No. PNUNA-SE-04, 1990.
23. D.K.Hart, S.E.Rutherford and A.H.S. Wickham, "Structural Reliability Analysis of Stiffened Panels", Trans. RINA, 1985.
24. ABS; Rules for Building and Classing Steel Vessels, 1987.
25. J.K.Paik and G.Kim, "Estimation of the Ultimate Compressive Strength of Actual Ship Panels with Complex Initial Deflection", J. of Society of Naval Architects of Korea, Vol.25, No.1, 1988 (in Korean).
26. S.P.Timoshenko and J.M.Gere, Theory of Elastic Stability, Second Edition, McGraw-Hill, 1963.
27. Y.Ueda, S.M.H.Rashed and J.K.Paik, "Effective Width of Rectangular Plates Subjected to Combined Loads", J. of Society of Naval Architects of Japan, Vol. 159, 1986 (in Japanese).
28. J.K.Paik, "An Analytical Solution of Nonlinear Behaviour for Simply Supported Rectangular Plates Subjected to Biaxial Compression", Proc. of the Autumn Symposium of Korea Ship Structure Congress, Society of Naval Architects of Korea, 1990 (in Korean).
29. J. Rhodes, "Effective Widths in Plate Buckling", in Developments in Thin-Walled Structures, Edited by J.

Rhodes and A.C. Walker, Applied Science Publishers, 1982.

30. Y.Ueda et.al., "Ultimate Strength of Square Plates Subjected to Compression (1st Report) - Effects of Initial Deflection and Welding Residual Stress -", J. of Society of Naval Architects of Japan, Vol.137, 1975 (in Japanese).
31. J.K.Paik and C.Y.Kim, "A Simplified Finite Element Method for the Ultimate Strength Analysis of Plates with Initial Imperfections", J. of Society of Naval Architects of Korea, Vol.26, No.1, 1989.
32. T.Usami et.al., "Tests on the Interaction Strength Between Local and Overall Buckling of Welded Box Columns", J. of Society of Civil Engineering of Japan, Vol.308, 1981 (in Japanese).
33. J.K. Paik, "Ultimate Longitudinal Strength-Based System Safety Assessment of a New Suezmax-Sized Double Skin Tanker", J. of Society of Naval Architects of Japan, Vol.169, 1991 (to be Appeared).
34. M. Kmiecik, "Factors Affecting Load-Carrying Capacity of Plates", Scientific Proceedings No.115/4, Shipbuilding Institute, Szczecin Technical University, 1981.
35. J. Czujko, "Collapse Analysis of Plates Subjected to Biaxial Compression and Lateral Load", Norwegian Institute of Technology, University of Trondheim, Norway, Nov., 1983.
36. T. Jastrzebski, "Allowable Distortions in Shipbuilding Plates -Some Technical Aspects-", Bulletin Technique du Bureau Veritas, No.4, 1988.